https://doi.org/10.5194/egusphere-2022-217
Preprint. Discussion started: 12 May 2022

Drone-towed CSEM system for near-surface geophysical prospecting: On instrument noise, temperature drift, transmission frequency and survey setup

Tobias Bjerg Vilhelmsen and Arne Døssing

Crustal Magnetism Technology and Research Group, DTU Space, Technical University of Denmark, Centrifugevej 356, 2800 Kgs. Lyngby, Denmark.

Correspondence: Tobias Bjerg Vilhelmsen (tobjer@space.dtu.dk)

Abstract. Drone-borne controlled source electromagnetic (CSEM) systems combine the mobility of airborne systems with the high subsurface resolution in ground systems. As such, drone-borne systems are beneficial at sites with poor accessibility and in areas where high resolution is needed, e.g., for archaeological or subsurface pollution investigations. However, drone-borne CSEM systems are associated with challenges, which are not observed to same the degree in airborne or ground surveys. In this paper, we explore some of these challenges based on an example of a new drone-towed CSEM system. The system deploys a multi-frequency broadband electromagnetic sensor (GEM-2UAV), which is towed six meters below a drone in a towing-bird configuration together with a Novatel GNSS-IMU unit, enabling centimetre level position precision and orientation. The results of a number of controlled tests of the system are presented together with data from an initial survey at Falster (Denmark), including temperature drift, altitude vs signal, survey mode signal dependency, and the effect of frequency choice on noise. The test results reveal the most critical issues for our system and issues that are likely encountered in similar drone-towed CSEM setups. We find that small altitude variations (+/- 0.5m) along our flight paths drastically change the signal, and a local height vs signal correlation is needed to correct near-surface drone-towed CSEM data. The highest measured impact was -46.2ppm/cm for a transmission frequency of 91kHz. We also observe a significant increase in the standard deviation of the noise level up to 500% when going from one transmission frequency to five. We recommend not to use more than three transmission frequencies, and the lowest transmission frequencies should be as high as the application allows it. Finally, we find a strong temperature dependency (up to 32.2ppm/C), which is not accounted for in the instrumentation.

https://doi.org/10.5194/egusphere-2022-217
Preprint. Discussion started: 12 May 2022

1 Introduction

Small uncrewed aerial vehicles (drones) are becoming increasing more popular survey platforms (instrumental carriers) for geophysical and archaeological prospecting, and a vast amount of applied geophysical studies use different types of sensors as part of a drone-borne systems. Among others, drones are used as an instrumental carrier for ground penetration radar studies (Altdorff et al., 2014), gamma-ray studies (Mochizuki et al., 2017), thermal investigations (Poirier et al., 2013; Petzke et al., 2013), LiDaR (Risbøl and Gustavsen, 2018), and magnetic investigations (Eppelbaum and Mishne, 2011; Petzke et al., 2013; Døssing et al., 2021; Schmidt and Coolen, 2021; Kolster et al., 2022). In general, electromagnetic induction methods are among the most commonly used techniques for mineral exploration but are, to our knowledge, not commonly used as a drone-borne system. Some studies working with drone-borne electromagnetic systems (Karaoulis et al., 2020; Mitsuhata et al., 2022), e.g., use the GEM2-UAV from geophex to measure the electromagnetic response from the subsurface. One alternative method to this approach is the semi-airborne solution described in Kotowski et al. (2022), where the transmitter is placed on the ground instead of transporting the transmitter together with the receiver on the drone. As drone-borne solutions are still advancing, we here strive to further push the investigation of drone-borne solutions with electromagnetic sensors.

Controlled source electromagnetic (CSEM) systems and techniques are popular in both airborne and handheld applications while drone-borne CSEM systems are, as mentioned before, less common. Large airborne CSEM systems, typically by helicopter (heliborne), can cover large areas quickly and effectively and are mainly associated with large-scale geophysical prospecting (Siemon et al., 2009). Handheld applications are typically associated with small-scale geophysical prospecting using a smaller instrument coil size, which - combined with a low operation height - produces high spatial resolution of near-surface targets. The modern CSEM sensor systems, both for heliborne and handheld applications, are complex and highly suited for each specific application with different pros and cons. While handheld versions lack mobility, i.e. wetlands, lakes, or overgrown areas are difficult to map, heliborne systems are highly mobile but are also more costly and provide lower spatial resolution due to increased survey height.

A handheld instrument mounted on drones can improve mobility and increase the range of access with the same spatial resolution as handheld surveying at an affordable price. However, the drone platform introduces several technical challenges, particularly related to the drone's electromagnetic noise and the undesired movement of the sensors during flight, both of which can reduce the quality of the data if not accounted for. The electromagnetic noise from the drone becomes an issue when the drone and the CSEM sensor are too close, since the sensor is unable to separate the electromagnetic response from the subsurface from the electromagnetic signal/noise from the drone. One possible solution for reducing noise is a towed bird system, which is often used for airborne systems that deploy electromagnetic sensitive sensors. A towed bird system is essentially a wire configuration that connects the instrumentation with the instrument carrier (drone or helicopter), which allows the instrumentation to be towed at a certain distance underneath the platform during flight. A towed bird configuration, however, introduces undesirable oscillations and movements of the instrument; something that needs to be precisely monitored and

https://doi.org/10.5194/egusphere-2022-217
Preprint. Discussion started: 12 May 2022

recorded by GNSS and IMU sensors on-board the bird (Kolster et al., 2022).

When dealing with CSEM instrumentations, we operate with a transmitting and receiving coil. A theoretical description of the coils and the electromagnetic field has been well described in various textbooks (e.g., Ward and Hohmann, 1988; Telford et al., 1990; Kaufman and Hoekstra, 2001; Everett, 2013), which explain several techniques and geometrical configurations for a set of coils that can be employed in geophysical prospecting. In this context, Ward and Hohmann (1988) present a beneficial description of the electromagnetic behaviour for finite sources over a layered half-space and provide expressions for coils separated by a distance above a layered subsurface. The expressions by Ward and Hohmann (1988) also include the height above the surface, which changes during flight for a drone-borne system. In addition, the towed bird oscillates in pitch, heading, and roll, providing an individual height change for the receiving and transmitting coils. This influences the readings significantly when flying close to a surface.

Here, we focus on a bistatic multi-frequency configuration. We present our findings for a drone-towed CSEM system and highlight some precautions that should be taken when collecting data. We use the controlled-source electromagnetic induction sensor GEM-2UAV from Geophex (Lerssi et al., 2016). Our approach is tuned to achieve the highest possible quality of data for near-surface archaeological prospecting. Still, our results can also be used for other targets in the subsurface. We present tests concerned with instrument noise, temperature drift, transmission frequency, and survey setup. These tests enable us to clarify - and correct for - some of the visual irregularities in our drone data. We include our recommendations for producing high data quality for drone-borne CSEM systems.

https://doi.org/10.5194/egusphere-2022-217
Preprint. Discussion started: 12 May 2022

2 Method

As part of the method, we introduce the CSEM sensor in Section 2.1, followed by the description of our drone-towed system in Section 2.2. When we combine the CSEM sensor with the drone-towed system, we refer to it as a drone-towed CSEM system. Section 2.3 describes some tests conducted with the CSEM sensor alone as well as test conducted with the drone-towed CSEM system. The purpose of the tests is to clarify some of the unwanted features in the CSEM survey data. Finally, in Section 2.4, we describe how we typically plan and execute surveys with the drone-towed CSEM system, and as a case study, we explain how it was used in a test site near Virket at Falster, Denmark.

2.1 CSEM sensor (GEM-2UAV)

Documentation of the GEM-2UAV is sparse. However, the instrument shares most of its features with the handheld version GEM-2 for ground surveys (Lerssi et al., 2016), which has been shown to be useful for archaeological prospecting (Tang et al., 2018). Other CSEM sensors of interest for near-surface prospecting include the Dualem-1S, EM38, or Profiler 400-EMP (Abdu et al., 2007; Bjella et al., 2010). Among these and other instruments, the GEM-2UAV was selected because it is lightweight and has a multi-frequency setting.

The GEM-2UAV can operate at up to ten frequencies between 25 Hz and 96 kHz simultaneously and it weighs approximately 3 kg, excluding a battery and positioning system. Operating the GEM-2UAV requires a suited battery, a GNSS antenna and the WinGEM software installed on a laptop. In terms of power consumption, the GEM-2UAV requires 18-28V and consumes 20W during surveying (transmission mode), and less than 2.5W during standby mode. The instrument has an input plug for GNSS antenna connection, with a baud rate of 9600 and word format of 8 Data Bits, 1 Stop bit, and "None" hardware flow control (9600, 8, 1, N).

The GEM-2UAV is shaped like a ski with a receiving (Rx) and transmitting (Tx) coil located at each end, 1.6 meters apart. This is named a "bistatic" configuration, which allows us to survey in different "modes", where P- and T-mode indicate whether the ski is aligned or transverse with the survey direction, respectively, and the vertical and horizontal coplanar mode indicates whether the coils are levelled vertically or horizontally. The latter should not be confused with the horizontal or vertical dipole-dipole configuration, which also deals with coil configurations but refers to the coil's magnetic or electrical dipole moment. Our tests and surveys only operate the sensor in the horizontal coplanar mode. Nonetheless, when flying with the sensor, we expect a little oscillation and rotation, which has an impact on the assumption of a perfect horizontal coplanar mode.
Before starting a survey with the GEM-2UAV, it needs to be initialised and set to log the data. This is achieved by connecting to the GEM-2UAV's control unit, which also provides the option of choosing the transmission frequencies and the length of the median filter, located on top of the ski. Once these operating options has been chosen, the GEM-2UAV's transmission mode is switched on, and data logging starts.

https://doi.org/10.5194/egusphere-2022-217
Preprint. Discussion started: 12 May 2022

The raw data extracted from the GEM-2UAV are in-phase and quadrature responses in parts-per-million (ppm). These in-phase and quadrature data are the real and imaginary part of the ratio between the magnetic intensity fields from the receiving coil (H_s) and transmitting coil (H_p). A discussion of the different ways of expressing this field ratio is outside the scope oof this paper, but it is useful for the subsequent discussion to state it as described in Ward and Hohmann (1988):

$$\frac{H_s}{H_p} = r^2 \int_0^\infty \frac{u-\lambda}{u+\lambda} \lambda e^{-2\lambda h} J_1(\lambda r) d\lambda \tag{1}$$

Where r is the distance between coils, h is the height above the surface, J_1 is the Bessel function of the first order, λ is called the separation constant ($\lambda = \sqrt{(k_x^2 + k_y^2)}$), u is the modified wavenumber ($u = \sqrt{(\lambda^2 - k^2)}$) where k is the wavenumber. The wavenumber is assumed to be $i\omega\mu\sigma$ in our application for low frequency domains, where μ is magnetic permeability, μ_0 is the free-space permeability, σ is the electrical conductivity, and ω is the angular frequency with the relation $\omega = 2\pi f$ to the transmission frequency f.

The expression in Eq. 1 is frequently used in airborne EM applications in which the survey height is an essential parameter. The expression also enables us to convert in-phase and quadrature ppm-values into the apparent electrical conductivity and magnetic susceptibility, respectively (Huang and Fraser, 2000, 2001, 2002). It should be noted that the susceptibility is most prominent in the in-phase response at lower transmission frequencies (Won and Huang, 2004), i.e. it is valuable, for near-surface applications, to have both the quadrature response from high transmission frequencies and the in-phase response from low transmission frequencies as this enables us to precisely calculate susceptibility and conductivity for near-surface targets.

The default median filter uses three data points, which means it will output data at sampling $\frac{\text{Sampling rate}}{\text{median filter}} = \frac{25}{3}$Hz. However, there is plenty of space on the 32Gbit SD card to store raw, unfiltered data, even for a full day of surveying, thereby allowing the user to conduct the preferred filtering of the data instead. In addition to the actual data output, the GEM-2UAV conveniently also stores a ppm-value for the local power line amplitude, which indicate how affected the data are by the local power grid.

The sensor can use up to ten transmitted frequencies. Still, the factory only recommends using five or fewer transmitted frequencies for which the skin depth $D = \frac{1}{\sqrt{\pi\mu\sigma f}}$ is convenient in a simple estimation of the depth of penetration (Huang, 2005).

2.2 Drone-towed system

The drone-towed system consists of three main parts: the drone, the suspension system, and the towing bird setup, which also houses the GEM-2UAV sensor (Figure 1).

For survey drone, we used the off-the-shelf DJI Matrice 600 Pro, which has a maximum recommended payload of 15.5 kg

https://doi.org/10.5194/egusphere-2022-217
Preprint. Discussion started: 12 May 2022

and a flight time of approximately 20 minutes with the survey setup. The Matrice 600 Pro is equipped with real-time kinematic positioning (RTK), which includes ground station communication with the drone by radio link.

The suspension system is the DTU-patented sensor suspension system (Døssing and Jakobsen, WIPO Patent Application No. 2017EP68246. 2018), in which a pulley system keeps the towing bird levelled and its direction constant during surveying. Based on the knowledge gained, which we discuss later, the length of the suspension system was set to 6m.

The towed bird consists of as a semi-rigid frame, which carries the CSEM sensor and a battery as well as an external, high-precision Novatel GNSS-IMU and logging device for precise positioning and 3D altitude information. The frame is constructed out of non-conductive fibreglass and 3D printed plastic, which allows us to separate the GNSS-IMU, logging device and battery from the CSEM sensor, thereby reducing the electromagnetic noise. The 3D printed parts of the frame ensure a flexible design, which proved to be extremely valuable during the initial developmental phase. The 3D printed setup also allows the CSEM sensor to be easily replaced if a superior sensor becomes available. The total weight of the towing frame, battery, high-precision GNSS-IMU and logging device is 2 kg; combined with the 3 kg CSEM sensor, the precisely positioned drone-towed CSEM system weighs 5 kg in total.

[Figure 1 around here.]

2.3 Tests

Following completion of the drone-towed CSEM system and initial flight tests, we encountered some irregularities in the data, which had not previously been identified for the handhold applications. In order to investigate the cause of these irregularities, we performed a series of tests on both the CSEM sensor itself and on the drone-towed CSEM system as a whole:

Test 1 - P- and T-mode: A handheld walking survey was performed across a metal target with a strong electromagnetic response. The test was repeated twice while pointing the instrument in different directions; First in P-mode, pointing the GEM2-UAV ski parallel to the survey direction, and next in T-mode, pointing the GEM2-UAV perpendicular to the survey direction. The goal of the P- and T-mode test was to evaluate the sensitivity of the sensor and the difference in the positioning of a small target with precisely known positioning.

Test 2 - Temperature drift: In this test, we compared the ambient temperature with changes in output ppm-values from three transmitted frequencies. The measurements were conducted in a quiet electromagnetic environment, in which the instrument was subjected to temperature changes by exposing it to direct sunlight or by shading it from sunlight. The duration of the test was 1.5 hours, during which the instrument did not move and was not manipulated in any way. The purpose of the temperature drift test was to evaluate the sensitivity of the sensor to temperature changes.

Test 3 - Height above surface correlation - Static: We tested the change in ppm-values for different heights above the surface. In a series of static tests, the instrument measured for at least three minutes at fixed XY-position but at different

https://doi.org/10.5194/egusphere-2022-217
Preprint. Discussion started: 12 May 2022

heights for every three minutes. This was achieved by suspending the instrument by two wires between two trees. By pulling the wires, the height above the surface could be adjusted. The purpose of this test was to provide direct information about the height versus signal correlation as we expected the drone to be unable to maintain a constant (within centimeters) flight altitude throughout a survey.

Test 4 - Noise effect of multiple transmitted frequencies: Initial tests with the GEM-2UAV indicated a significant correlation between noise and the number of transmitted frequencies. The goal of this test was, therefore, to illustrate the dependency of instrumentation noise on the number of transmitted frequencies. The test consisted of five independent sub-tests, each of which had the following transmission frequencies:

1. 475Hz alone
2. 91.275Hz alone
3. 475Hz and 91.275Hz together
4. 475Hz, 23.175Hz, 45.875Hz, 68.575Hz, and 91.275Hz together
5. 475Hz, 10.575Hz, 20.675Hz, 30.725Hz, 40.825Hz, 50.925Hz, 61.025Hz, 71.075Hz, 81.175Hz, and 91.275Hz together

For all measurements, the instrument was placed in a fixed position one meter above the surface and in an area with low electromagnetic noise. We evaluated the noise by calculating the standard deviation for a low transmitted frequency (475Hz) and a high transmitted frequency (91.275Hz) from each of these independent sub-tests. Each of the tests lasted for more than three minutes.

Test 5 - Noise effect of spacing between transmitted frequencies: Another noise investigation test was performed; this time it was designed to investigate how the separation between two transmitted frequencies changes the instrumentation noise. We paired up two transmitted frequencies and calculated the standard deviation for 475Hz and 91.275Hz. The pairs we used were as follows:

- The standard deviation of the transmitted frequency 475Hz using the pairs; (475Hz and 91.275Hz), (475Hz and 23.175Hz), (475Hz and 45.875Hz), and (475Hz and 68.575Hz)
- The standard deviation of the transmitted frequency 91.275Hz using the pairs; (91.275Hz and 475Hz), (91.275Hz and 23.175Hz), (91.275Hz and 45.875Hz), and (91.275Hz and 68.575Hz)

Test 6 - Noise from drone: The aim of this final test was to evaluate the noise from the drone in a convincing but straightforward way to find a threshold at which point the drone is no longer visible in the output ppm-values. We conducted the test for a transmitted frequency of 475Hz and 93.075Hz individually. The test was conducted by hovering the drone at a certain altitude for at least one minute and evaluating the standard deviation of the data.

https://doi.org/10.5194/egusphere-2022-217
Preprint. Discussion started: 12 May 2022

2.4 Drone-towed CSEM study at Falster, Denmark.

A drone-towed CSEM test survey was carried out at Falster, Denmark. The study site is close to the town of Virket, which has received a lot of attention recently since what is believed to be the biggest Viking fortress discovered in Denmark is located there (TV2Øst, 2020). The total area of the site is 78.000 m^2, of which half is a golf course and the other half is a field. The area has a 5m embankment on three sides. Planning and conducting a survey requires a lot of thought, but the structure and terminology are very similar for ground and airborne surveys. Figure 2 below, is an illustration of a simple survey design. A similar approach was used for the Falster study.

[Figure 2 around here.]

A drone-borne LiDaR topography survey was conducted to produce a precise local topography model of the survey area. The topography model was included in the drone flight planning software, UgCS, and the drone was set to fly at an altitude, which resulted in a distance between the sensor and the surface of 1m. The survey line spacing was set to 0.5m, with a 5m overshoot at the ends. Based on the outcome of the P-mode versus T-mode test (Test 1), we conducted the Falster survey with a constant heading in T-mode configuration, i.e., the sensor always pointed in the same direction (the CSEM Tx-coil, for the given survey, pointed in a north-easterly direction). Since it was being towed 6m underneath a drone in a suspension system, the sensor was not expected to have a completely straight path, as seen in the ideal case in Figure 2. Therefore, a lot of effort was put into post-processing the GNSS and IMU positioning information of the system with NovAtel software (NovAtel Inc.). Post-processing enables knowledge of the sensors positioning and orientation down to the level of centimetres. Data in overshoot, landing, and take off were removed.

3 Results

This section uses the raw ppm-values from the CSEM sensor. We compare the test results with the standard deviation of the Falster study (Table 1C). The expectation is that the standard deviation of the Falster study will indicate a typical response from the subsurface. It should be noted that similar results concerning the standard deviation of a flight survey were made in previous investigations for a different study site in Denmark (Bjerg et al., 2020). Additionally, Table 1 contains numbers concerning temperature, height above the surface and the correlation between height and ppm-values for the Falster study. The numbers in Table 1 are meant to collect and clarify essential issues of the results.

3.1 Test results

Figure 3 shows the measurements from Test 1. The data is the sum of the quadrature response with the transmitted frequencies of 475Hz, 1525Hz, 5325Hz, 18325Hz, and 63025Hz. Figure 3a shows measurements in P-mode while Figure 3b shows measurements in T-mode. The heavy metal object, which is placed in the centre of the survey to show the response in P- and T-mode, is visible in the form of high peaks in the data for three adjacent survey lines in both modes. A black square encloses the data containing these peaks. Even though we might expect the peaks to be aligned across the survey lines, both P- and T-mode

https://doi.org/10.5194/egusphere-2022-217
Preprint. Discussion started: 12 May 2022

contain misalignment across adjacent lines. The peak-values are shifted along the survey lines by approximately 10m and 1.5m in P- and T-mode, respectively, i.e., each datapoint is shifted by about 5m and 0.75m forward in the survey direction to align in P- and T-mode, respectively. If it is assumed that the misalignment entirely due to a delay in timestamping, it corresponds to a delay of 0.24sec and 2.04sec for P- and T-mode, respectively, based on an estimated data point shift of 2 and 17 points with the known sampling rate of 8.3Hz.

Another interesting outcome of the P- and T-test is the difference in the amplitude of the recorded signal. The target response has a stronger peak-value for the adjacent lines when using T-mode, which suggests a stronger response from targets across the survey line when surveying in T-mode.

[**Figure 3** around here.]

The results of the temperature drift Test 2 are visualised in Figure 4. Figure 4a and 4b show the temperature and inverse temperature in Celsius degree while Figure 4c to 4h show the corresponding ppm-values for three different transmitted frequencies. A clear correlation is seen between ppm-values and temperature. However, the correlation is less pronounced for the lower transmission frequencies. In this connection, the y-axis ranges, which are scaled individually, should be noted. We have calculated an estimated temperature effect per degree (Table 1A), for which we used the difference between the maximum and minimum ppm-values and temperatures. We observe that the temperature effect decreases with decreasing transmitting frequencies, even though the temperature effects from Table 1A at 40.045Hz appear negligible, the temperature effects are still visible in Figure 4.

[**Figure 4** around here.]

The results of Test 3 are shown in Figure 5, in which the dependency between height above ground and the ppm-value is demonstrated. The CSEM sensor is recording above the same spot but at 12 different heights between 10cm and 130cm above the surface. The red lines in Figure 5 represent a linear fit to the data. Note that the fit does not have the same slope or interception with the y-axis for any of the frequencies. The slopes of the individual fits are listed in Table 1. We conducted this test at different locations, which produced different slopes and interceptions, but all with a linear trend. Although the linear fit is not a perfect representation of the height dependency, it provides a useful first approximation and indicates the correlation between height above ground and the ppm-value.

[**Figure 5** around here.]

[**Table 1** around here.]

In Figure 6 and Figure 7, we present the results of Test 4 and Test 5, which are related to the calculated standard deviation for different combinations of transmitted frequencies and for different spacing between transmitted frequencies. Figure 6, illustrates how the standard deviation is highly dependent on the number of frequencies. The standard deviation for 91.275Hz with the additional 475Hz ranges from a standard deviation of ~ 20 to ~ 60 while the effects on 475Hz having any additional

https://doi.org/10.5194/egusphere-2022-217
Preprint. Discussion started: 12 May 2022

transmission frequency are negligible. Adding, e.g., three frequencies between 475Hz and 91.275Hz will have an effect on both the 475Hz and 91.275Hz frequencies, with the strongest effect at 91.275Hz (Figure 6). For five transmitted frequencies, the standard deviation ranges from 73 to 102, where a standard deviation of 73 is the smallest value for all five transmitted frequencies. As seen in Figure 7, we further observe that the spacing between the frequencies has a strong effect on the output noise level. This is particularly evident when pairing high frequencies (e.g., 91.275 Hz) with lower frequencies; an effect that was observed to increase as the spacing between the frequencies increased. Here, it may be of value to compare with the standard deviation from the Falster study in Table 1C, in which the noise from 475Hz, 1.525Hz, and 5.325Hz is close to 73, indicating that the noise from the number of frequencies and frequency spacing is the main signal in the Falster study for these frequencies. In contrast, a standard deviation of 478.6 in the quadrature response in the Falster study is a promising signal to noise ratio.

[**Figure 6** around here.]

[**Figure 7** around here.]

Table 2 lists the results of Test 5, which are related to the noise effect of distance to the drone. The table lists the calculated standard deviation of the ppm-values collected with the drone hovering above the CSEM sensor at different altitudes. The effect of the drone is negligible above 5.2m while a significant noise effect is observed at shorter distances. At a distance of 0.3m, i.e., the sensor is mounted on the drone landing gear, the standard deviation increases a factor 30. This is almost a 3000% increase in standard deviation compared to the 5.2m scenario. For the results in the Falster study (see below), we used a distance of 6m to ensure that the effect from the noise from the drone was negligible.

[**Table 2** around here.]

3.2 Drone-towed CSEM study at Falster, Denmark

Figure 8 shows the results of the Falster study made with the drone-towed CSEM. The figure displays the raw response from quadrature at 63025Hz in Figure 8a and in-phase at 475Hz in Figure 8b. From the description in subsection 2.1 we would expect the response in Figure 8a to be dominated by conductivity and the response in Figure 8b to be dominated by susceptibility. The highlighted sub-area in Figure 8 is enlarged and shown in Figure 9. Note that the ppm-values between the adjacent and overlapping survey lines are generally inconsistent.

[**Figure 8** around here.]

[**Figure 9** around here.]

In Figure 10, we show a scatter-density plot of the raw ppm-value vs altitude for the Falster study. As seen, the majority of the measurements are at one meter above ground +/- 0.5 meters. Least-square fits to the data in Figure 10 are also shown based on the expression $a + b \cdot \exp(h \cdot c)$, where h is the altitude, and a,b, and c are the optimised parameters. Reasonable fits are

https://doi.org/10.5194/egusphere-2022-217
Preprint. Discussion started: 12 May 2022

observed for both the quadrature and in-phase data. In Figure 11, we show the fits for all the frequencies. We do not see a perfect linear dependency as we observed in the results of Test 3 (Figure 5). It is apparent from Figure 11 that the quadrature responses are very sensitive to altitude change, in particular, at the high frequencies (18325Hz, 63025Hz) while the in-phase response is generally less affected as soon as the altitude is above 1m. For the quadrature response at 63025Hz, the change from 0.5m to 1.5m is 1600ppm resulting in approximately 16ppm/cm, while for the in-phase at 63025Hz, the same change in altitude results in a change in response of 280ppm. All the estimated parameters and the calculated standard deviation for the Falster survey are listed in Table 3.

[**Figure 10** around here.]

[**Figure 11** around here.]

[**Table 3** around here.]

Figure 12a and b show the ppm-values from the quadrature response at 63025Hz and the in-phase response at 475Hz after correcting for the altitude dependency. The time delay was small, and we found no visible effect by including a delay. Figure 12 can be compared to Figure 8 as a before and after altitude correction. As seen, the altitude corrected data for the quadrature response (Figure 12a) is significantly smoother than without the altitude correction (Figure 8a). Even though the in-phase response at 475Hz is treated in the same way, we found no visible improvement between Figure 8b and Figure 12b. Similar altitude correlation was examined for all data, but the quadrature response at 63025Hz was the only one that exhibited an improvement.

[**Figure 12** around here.]

https://doi.org/10.5194/egusphere-2022-217
Preprint. Discussion started: 12 May 2022

4 Discussion

In the paper, we present a drone-towed CSEM system, where the choice of CSEM sensor was mainly limited by the payload capabilities of the available survey drone. A more powerful drone would allow the use of different instrumentation but would also come at the expense of greater noise and higher costs. Ultimately, a light payload increases flight time per battery, which is desirable regardless of the drone.

The system presented in this study is based on a towed CSEM sensor. An alternative way of constructing a drone CSEM system is to mount the sensor directly under the drone. However, as seen in Table 1, this would generate between 28 and 8 times more noise in the data. Therefore, based on the results presented here, it is not a question of whether or not to use a towed CSEM system, but rather a question of how to overcome the challenges associated with swaying of such a suspension system.

An alternative to the wire-based towing solution presented in this study is provided by Karaoulis et al. (2020), who use a rigid towing system and a bistatic sensor system like the GEM2UAV from Geophex. Whether a rigid suspension or a wire suspended CSEM system is beneficial is difficult to access without conducting a proper test. While a rigid suspension system most likely generates less unwanted swaying, its suspension length is constrained (and hence distance to the drone) and there are also difficulties related to landing.

In general, we consider the wire-based drone-towed CSEM system to be satisfactory, although we see possibilities for optimisation in a future version. In particular, the quality of the data may be improved by operating the system differently and providing more advanced post-processing of the data. We have tried handheld surveying with the same instrumentation, which resulted in more informative results and indicates that some of the noise observed in the drone-CSEM data is related to the pitch, heading, roll and altitude behaviour of the instrument when towed several meters below a drone. The effect of roll, pitch and heading is difficult to demonstrate since changes in these parameters will not produce a simple amplitude change in the measurement. On the contrary, they will create a different sensitivity profile in the subsurface (Tølbøll and Christensen, 2007) .

Currently, what effect roll, pitch, heading has is the biggest open question in our system. While we could not find any direct correlation between roll, pitch, heading and ppm-values, we are confident that changes in these parameters have an effect on our measurements, albeit not as a simple linear correlation. The roll, pitch, and heading are closely related to the altitude, which currently has the strongest effect on our data, as observed in Test 3 and in the Falster study. We observe a clear correlation between the altitude and the ppm-values. However, only for the quadrature response at 63025Hz does a correction for the altitude significantly improve the quality of the data (Figure 12). The altitude is rarely an issue when producing a handheld walking survey because the surveyor can maintain the instrumentation at approximately the same altitude throughout the survey. For heliborne surveys, the altitude is typically included in the processing, but the data - given the significantly higher survey altitude - is less affected by the orientation and the altitude of the instrument and therefore, it is sufficient to use one collective altitude for the system (like in Equation 1) and also to neglect the roll, pitch, and heading change. However, with

https://doi.org/10.5194/egusphere-2022-217
Preprint. Discussion started: 12 May 2022

a ppm-to-altitude correlation of ∼46 ppm/cm (Table 1) and a typical altitude change of +/- 0.5 meters during a near-surface (∼1m above the surface) drone survey, ignoring these effects becomes problematic. When a drone-towed CSEM sensor system moves close to the surface, any small changes in roll, pitch, and heading will have a strong effect compared to a heliborne system. While it would also be convenient to assume only one altitude measure, it seems insufficient for our application at low altitudes. If we were to numerically analyse this effect, we would need to treat each coil independently instead and abandon the generally accepted assumption of one altitude for both coils in the instrument (i.e., Equation 1). Hence, the roll, pitch, and heading effects may explain why we do not observe a linear altitude dependency in the Falster study as observed in the controlled altitude in Test 3.

In Figure 11b, we observe that the slope of ppm-values vs altitude converges to a similar response with decreasing frequencies. This effect arises from the relation to the wave number described in Won and Huang (2004), implying no dependence on either frequency or conductivity at low transmission frequencies for the in-phase response. It essentially means that the response is mainly real at low frequencies, while at high frequencies, the response is mainly complex. These observations become important when deciding on a set of transmission frequencies for a survey; if one wants to estimate both the magnetic susceptibility and the electrical conductivity, it is practical to have at least one high quadrature and one low in-phase frequency. In contrast, if one wants to estimate the layers in the subsurface, it is more convenient to have several frequencies in the same frequency region.

This brings us to the discussion on data noise and its dependency on frequency spacing and the number of frequencies (Figures 6 and 7). We found that the lowest transmitted frequency is not affected by one higher transmitted frequency whereas a lower transmitted frequency significantly affects a high transmitted frequency. This implies that the lowest transmitted frequency should always be carefully chosen, and it should not be lower than is absolutely necessary. Furthermore, the number of transmitted frequencies should be carefully selected as an increase in the number of transmitted frequencies contributes to greater noise, also for low transmitted frequencies. The user manual for the EM-instrumentation recommends no more than five transmitted frequencies, which is also obvious from Figure 6 in this study. However, even five transmitted frequencies may be too many, at least for drone-towed archaeological applications. The tests on noise and the Falster survey show that five transmitted frequencies produce too much noise, whereas two transmitted frequencies seems to be optimal. The lowest selected frequency should contain the most desired information while the highest should only contribute less critical information. In conclusion, it may be questioned whether it makes sense to have a multi-frequency CSEM-instrument, which allows ten possible transmitted frequencies when the noise seems to be already dominant for only five frequencies.

In terms of long wavelength instrumentation noise, a significant temperature drift, which was unrelated to any external electromagnetic sources, was observed in Figure 4. While the quadrature response has a positive correlation with temperature, the in-phase response has an overall negative - but still clearly visible - correlation with the temperature. We further noticed that the temperature affects the highest transmission frequencies the most. Temperature dependency is expected because a change

https://doi.org/10.5194/egusphere-2022-217
Preprint. Discussion started: 12 May 2022

in the temperature affects the resistivity of the sensor coils, which will then change the readings of the measurements. The temperature would probably not be an issue when conducting short field campaigns, but the temperature drift must be considered for a full day of fieldwork or field campaigns spread out over several days. It is possible to mount an external temperature sensor to measure temperature indirectly, which may be used to correct the data, although this is not ideal. Alternatively, a high-pass filter may level out any long-period temperature dependency.

Finally, it is important to mention the shift in peak-values between adjacent survey lines and the signal strength from the target across survey lines. In the handheld P- versus T-mode test survey in Figure 3, we can assume a close-to-constant instrument pitch, roll, and heading. All data points in the test were positioned using a Novatel GNSS-IMU system with centimeter-level precision. As observed in the test, 5 meters and 0.5-1 meters offset, respectively, were found between adjacent lines for the P- and T-mode surveys (Figure 3a); offsets that cannot be attributed to uncertainties in the GNSS-IMU. For now, these offsets are partly unaccounted for. When it comes to the signal strength from the P- and T-mode test in Figure 3, we further observed a broader, high-amplitude anomaly across survey lines in T-mode as compared to P-mode. This observation is consistent with the theoretical part for sensitivity for high induction numbers (Tølbøll and Christensen, 2007; Callegary et al., 2012). A heliborne EM system will have low induction numbers and, therefore, have a similar sensitivity signature in P- and T-mode. Thus, if drone-towed surveys are flown at higher altitudes or if only lower transmitted frequencies are used, the survey mode will not affect the data.

5 Conclusions

This paper has presented a drone-towed CSEM system and has identified precautions that need to be taken to reduce the noise in the raw data from a multi-frequency CSEM sensor, the GEM-2UAV from Geophex.

The drone-towed CSEM system is towed at an altitude of approximately 1m +/-0.5m above the surface and in a 6m wide-based suspension system below the drone. Because of the proximity to the ground, we observe that altitude changes at centimetre level are the main cause of variation in the data. While the altitude changes will contribute to an amplitude change in the response, the pitch, heading and roll change the sensitivity profile of the subsurface. This effect is, however, difficult to determine through measurements. However, one must consider including both the orientation and the altitude of the instrument to represent the response better, at least for low altitudes.

In addition to the strong altitude effect, we observe additional noise sources that have an effect on the system. Of particular importance is the spacing between - and the number of - transmission frequencies. The chosen CSEM sensor can be adapted to measure the magnetic susceptibility at low transmission frequencies or the electrical conductivity at high transmission frequencies. While it can measure at both ends of the frequency spectrum, it will generate a greater noise at the highest frequency. We recommend keeping the number of frequencies to a minimum, and the lowest frequency should not be lower

https://doi.org/10.5194/egusphere-2022-217
Preprint. Discussion started: 12 May 2022

than is absolutely necessary.

Finally, we observe a significant temperature dependency of up to 32 ppm/C^o. This long wavelength effect is not critical for the low frequencies or short duration surveys, but it may introduce notable errors in surveys conducted in environments with significant fluctuations in the ambient temperature.

Author contributions. TBV was in charge of planning the measurements, taking the measurements, processing the data and drafting the paper. AD was in charge of the overall direction, planning, and helping to finalise the paper.

Competing interests. The authors declare that they have no conflict of interest.

Acknowledgements. We want to thank Eduardo Lima Simões da Silva for assisting with the surveying and for his excellent work on the drone-towed system. Thanks to Leif Plith Lauritsen and the team at Museum Lolland-Falster it has been extremely helpful and insightful.

https://doi.org/10.5194/egusphere-2022-217
Preprint. Discussion started: 12 May 2022

References

Abdu, H., Robinson, D., and Jones, S. B.: Comparing bulk soil electrical conductivity determination using the DUALEM-1S and EM38-DD electromagnetic induction instruments, Soil Science Society of America Journal, 71, 189–196, 2007.

Altdorff, D., Schliffke, N., Riedel, M., Schmidt, V., van der Kruk, J., Vereecken, H., Stoll, J., and Becken, M.: UAV-borne electromagnetic induction and ground-penetrating radar measurements: a feasibility test, Water Resour Res, 42, W11 403, 2014.

Bjella, K. L., Astley, B. N., and North, R. E.: Geophysics for Military Construction Projects, Tech. rep., ENGINEER RESEARCH AND DEVELOPMENT CENTER VICKSBURG MS, 2010.

Bjerg, T., da Silva, E. L. S., and Døssing, A.: Investigation of UAV noise reduction for electromagnetic induction surveying, in: NSG2020 3rd Conference on Geophysics for Mineral Exploration and Mining, vol. 2020, pp. 1–5, European Association of Geoscientists & Engineers, 2020.

Callegary, J. B., Ferré, T. P., and Groom, R.: Three-dimensional sensitivity distribution and sample volume of low-induction-number electromagnetic-induction instruments, Soil Science Society of America Journal, 76, 85–91, 2012.

Døssing, A., Silva, E. L. S. d., Martelet, G., Rasmussen, T. M., Gloaguen, E., Petersen, J. T., and Linde, J.: A high-speed, light-weight scalar magnetometer bird for km scale UAV magnetic surveying: On sensor choice, bird design, and quality of output data, Remote Sensing, 13, 649, 2021.

Døssing, A. and Jakobsen: Suspension system patent, WIPO Patent Application No. 2017EP68246. 2018.

Eppelbaum, L. and Mishne, A.: Unmanned airborne magnetic and VLF investigations: Effective geophysical methodology for the near future, Positioning, 2, No. 3, 112-133, 2011.

Everett, M. E.: Near-surface applied geophysics, Cambridge University Press, 2013.

Huang, H.: Depth of investigation for small broadband electromagnetic sensors, Geophysics, 70, G135–G142, 2005.

Huang, H. and Fraser, D. C.: Airborne resistivity and susceptibility mapping in magnetically polarizable areas, Geophysics, 65, 502–511, 2000.

Huang, H. and Fraser, D. C.: Mapping of the resistivity, susceptibility, and permittivity of the earth using a helicopter-borne electromagnetic system, Geophysics, 66, 148–157, 2001.

Huang, H. and Fraser, D. C.: Dielectric permittivity and resistivity mapping using high-frequency, helicopter-borne EM data, Geophysics, 67, 727–738, 2002.

Karaoulis, M., Ritsema, I., Bremmer, C., and De Kleine, M.: Drone-Borne Electromagnetic (DREM) Surveying in The Netherlands, in: NSG2020 26th European Meeting of Environmental and Engineering Geophysics, 1, pp. 1–5, European Association of Geoscientists & Engineers, 2020.

Kaufman, A. A. and Hoekstra, P.: Electromagnetic soundings, vol. 34, Elsevier Science Limited, 2001.

Kolster, M. E., Wigh, M. D., Lima Simões da Silva, E., Bjerg Vilhelmsen, T., and Døssing, A.: High-Speed Magnetic Surveying for Unexploded Ordnance Using UAV Systems, Remote Sensing, 14, 1134, 2022.

Kotowski, P. O., Becken, M., Thiede, A., Schmidt, V., Schmalzl, J., Ueding, S., and Klingen, S.: Evaluation of a Semi-Airborne Electromagnetic Survey Based on a Multicopter Aircraft System, Geosciences, 12, 26, 2022.

Lerssi, J., Niemi, S., and Suppala, I.: GEM-2-New Generation Electromagnetic Sensor for Near Surface Mapping, in: Near Surface Geoscience 2016-22nd European Meeting of Environmental and Engineering Geophysics, 1, pp. cp–495, European Association of Geoscientists & Engineers, 2016.

https://doi.org/10.5194/egusphere-2022-217
Preprint. Discussion started: 12 May 2022

Mitsuhata, Y., Ueda, T., Kamimura, A., Kato, S., Takeuchi, A., Aduma, C., and Yokota, T.: Development of a drone-borne electromagnetic survey system for searching for buried vehicles and soil resistivity mapping, Near Surface Geophysics, 20, 16–29, 2022.

Mochizuki, S., Kataoka, J., Tagawa, L., Iwamoto, Y., Okochi, H., Katsumi, N., Kinno, S., Arimoto, M., Maruhashi, T., Fujieda, K., et al.: First demonstration of aerial gamma-ray imaging using drone for prompt radiation survey in Fukushima, Journal of Instrumentation, 12, P11 014, 2017.

Petzke, M., Hofmeister, P., Hördt, A., Glaßmeier, K., and Auster, H.: Aeromagnetics with an unmanned airship, in: Near Surface Geoscience 2013-19th EAGE European Meeting of Environmental and Engineering Geophysics, pp. cp–354, European Association of Geoscientists & Engineers, 2013.

Poirier, N., Hautefeuille, F., and Calastrenc, C.: Low altitude thermal survey by means of an automated unmanned aerial vehicle for the detection of archaeological buried structures, Archaeological Prospection, 20, 303–307, 2013.

Risbøl, O. and Gustavsen, L.: LiDAR from drones employed for mapping archaeology–Potential, benefits and challenges, Archaeological Prospection, 25, 329–338, 2018.

Schmidt, V. and Coolen, J.: Potential and Challenges of UAV-Borne Magnetic Measurements for Archaeological Prospection, Revue d'archéométrie, 45, 1, 2021.

Siemon, B., Christiansen, A. V., and Auken, E.: A review of helicopter-borne electromagnetic methods for groundwater exploration, Near Surface Geophysics, 7, 629–646, 2009.

Tang, P., Chen, F., Jiang, A., Zhou, W., Wang, H., Leucci, G., de Giorgi, L., Sileo, M., Luo, R., Lasaponara, R., et al.: Multi-frequency electromagnetic induction survey for archaeological prospection: Approach and results in Han Hangu Pass and Xishan Yang in China, Surveys in Geophysics, 39, 1285–1302, 2018.

Telford, W. M., Telford, W., Geldart, L., and Sheriff, R. E.: Applied geophysics, Cambridge university press, 1990.

Tølbøll, R. J. and Christensen, N. B.: Sensitivity functions of frequency-domain magnetic dipole-dipole systems, Geophysics, 72, F45–F56, 2007.

TV2Øst: Local news covering the story on Falster, http://web.archive.org/web/20080207010024/http://www.808multimedia.com/winnt/kernel.htm, accessed: 2022-05-02, 2020.

Ward, S. H. and Hohmann, G. W.: Electromagnetic theory for geophysical applications, in: Electromagnetic Methods in Applied Geophysics: Voume 1, Theory, pp. 130–311, Society of Exploration Geophysicists, 1988.

Won, I. and Huang, H.: Magnetometers and electro-magnetomenters, The Leading Edge, 23, 448–451, 2004.

https://doi.org/10.5194/egusphere-2022-217
Preprint. Discussion started: 12 May 2022

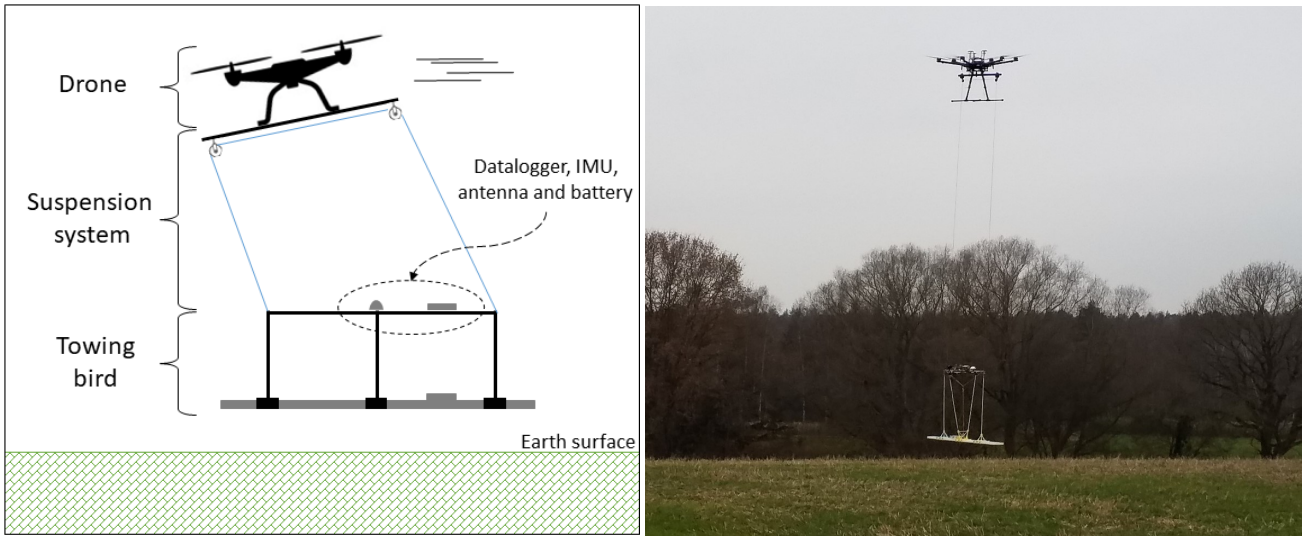

Figure 1. An illustration on the left of the drone setup and a picture from a field survey in Falster, Denmark.

https://doi.org/10.5194/egusphere-2022-217
Preprint. Discussion started: 12 May 2022

Figure 2. A sketch of a survey design where line spacing, survey heights, length of survey overshoot are some of the parameters that need to be considered when doing a CSEM survey.

https://doi.org/10.5194/egusphere-2022-217
Preprint. Discussion started: 12 May 2022

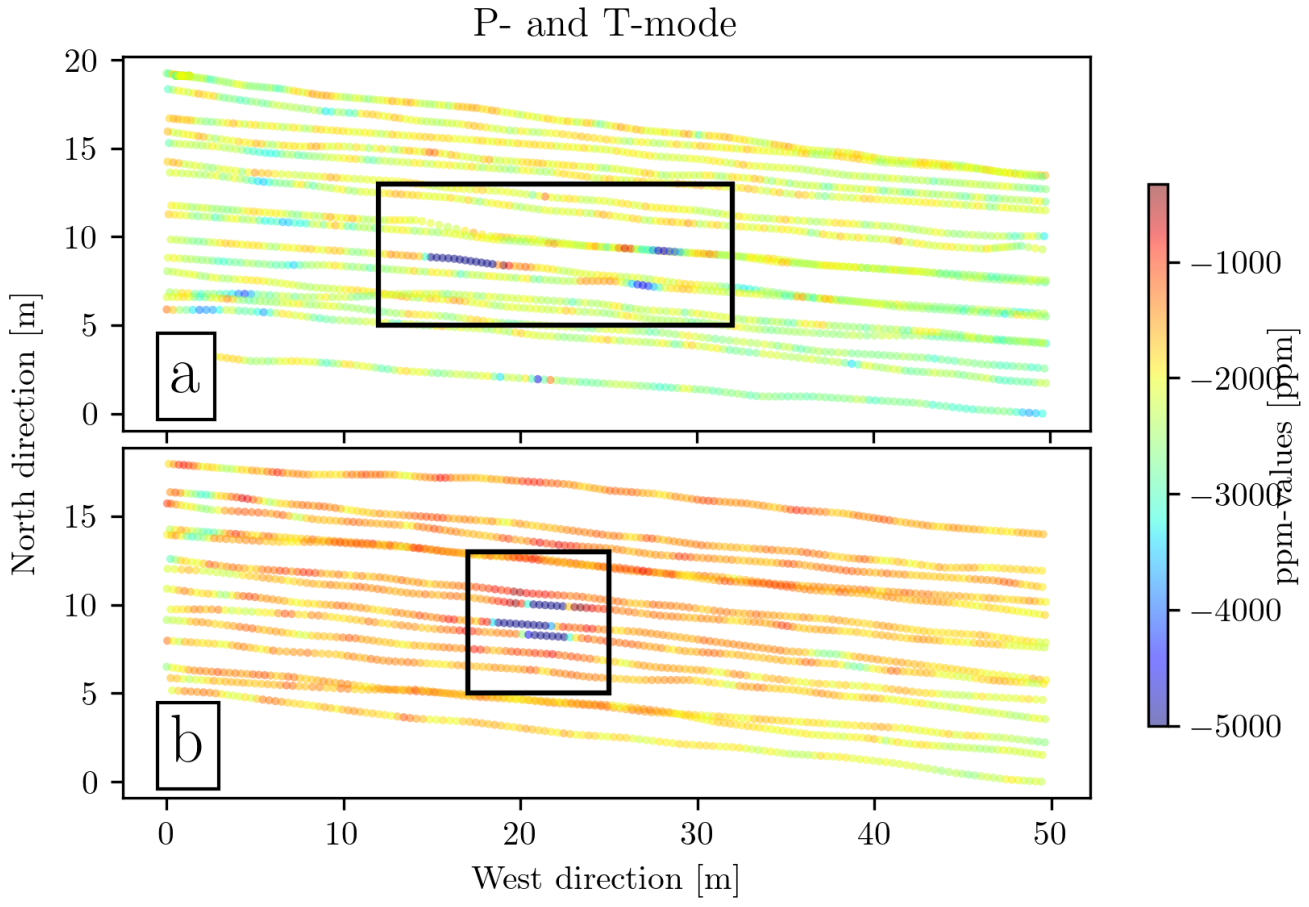

Figure 3. Results of Test 1. (a) P-mode, and (b) T-mode. A heavy metal object is placed in the centre of the survey; the black square encloses the area where it is observed in the data. The object is detected in three survey lines in both the P- and T-mode. Note that the P-mode has a distinctly higher peak anomaly value for the centre survey line compared to the two adjacent lines.

https://doi.org/10.5194/egusphere-2022-217
Preprint. Discussion started: 12 May 2022

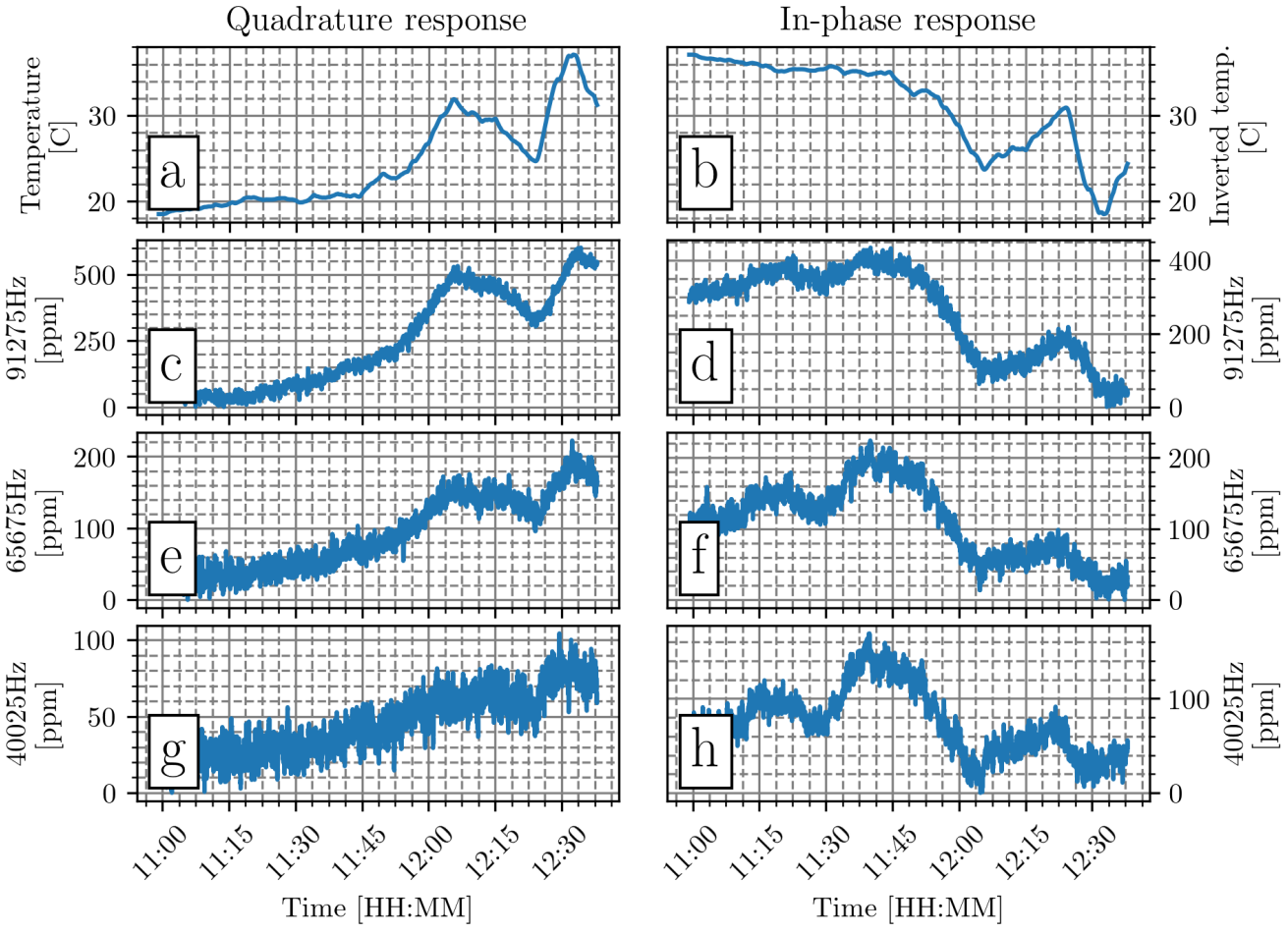

Figure 4. Results of Test 2: A static CSEM versus temperature measurement conducted in a quiet electromagnetic environment. The data is levelled to zero and processed with a median filter. (a) and (b) are the measured temperatures, but (b) is multiplied by -1 to invert the temperature for better comparison with ppm-observations for different frequencies in (c) to (h).

https://doi.org/10.5194/egusphere-2022-217
Preprint. Discussion started: 12 May 2022

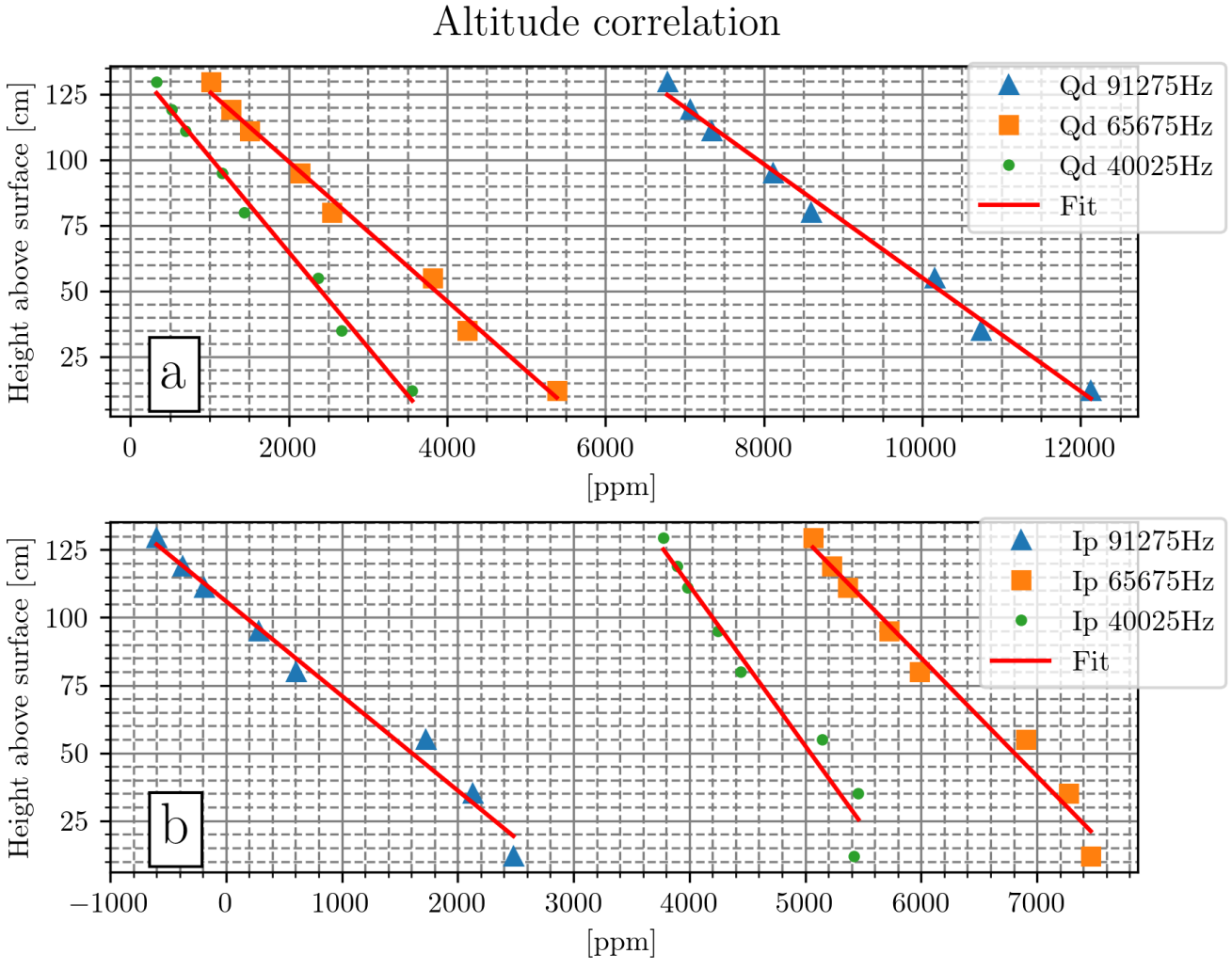

Figure 5. Results of Test 3 (measured ppm-values versus instrument altitude). Each measurement is a mean value of 3 minutes at each altitude. The Pearson correlation coefficient between altitude and ppm-values is in the range $[-0.98; -0.99]$.

https://doi.org/10.5194/egusphere-2022-217
Preprint. Discussion started: 12 May 2022

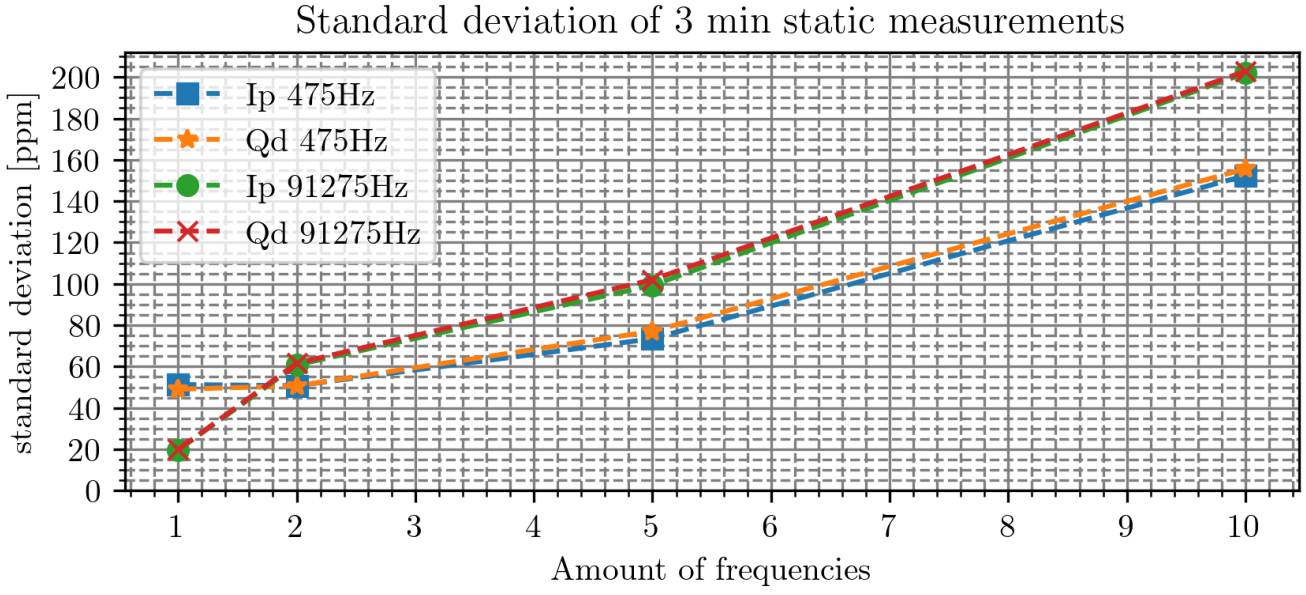

Figure 6. Results of Test 4. The calculated standard deviation for 475Hz and 91275Hz is shown with different number of transmitted frequencies. Note that when number of frequencies equals 1, it is the standard deviation on the frequency itself without any other transmitted frequencies. The additional frequencies between 475Hz and 91275Hz are linearly spaced.

https://doi.org/10.5194/egusphere-2022-217
Preprint. Discussion started: 12 May 2022

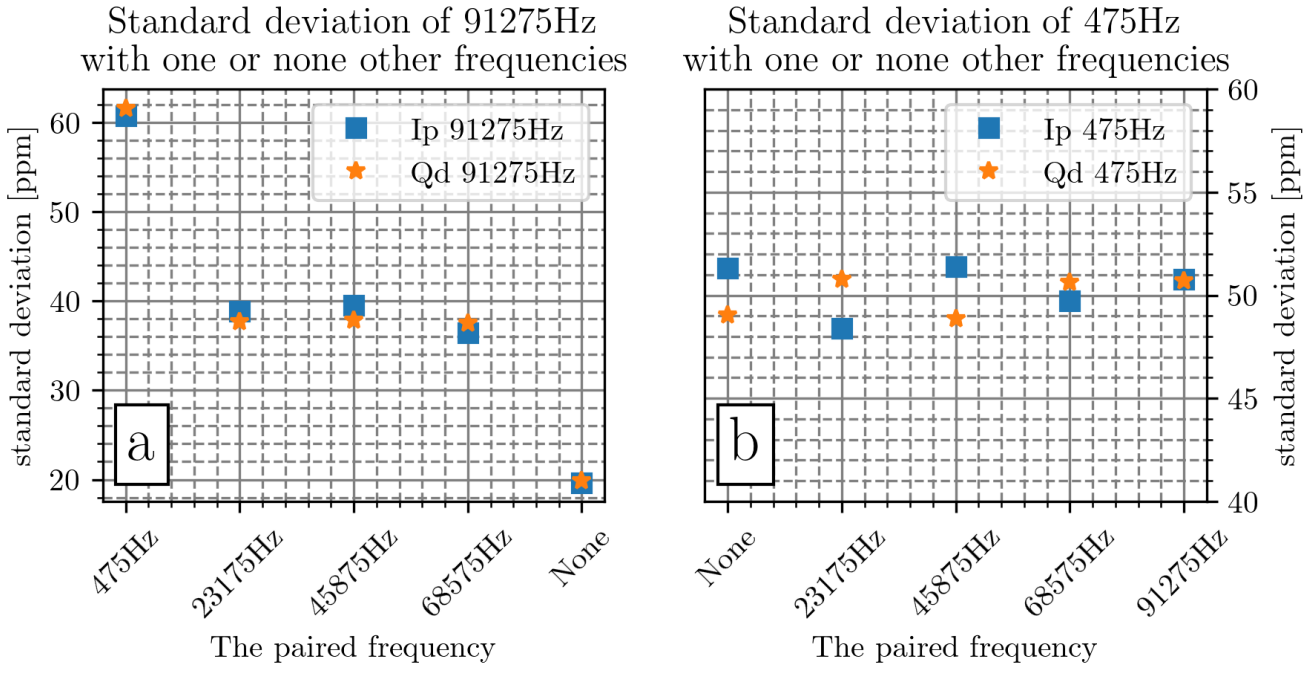

Figure 7. Results of Test 5. The standard deviation is calculated for 91275Hz and 475Hz with one additional transmitted frequency with decreasing spacing. Note that no notable effect is in 475Hz while the standard deviation in 91275Hz increases with increasing spacing.

https://doi.org/10.5194/egusphere-2022-217
Preprint. Discussion started: 12 May 2022

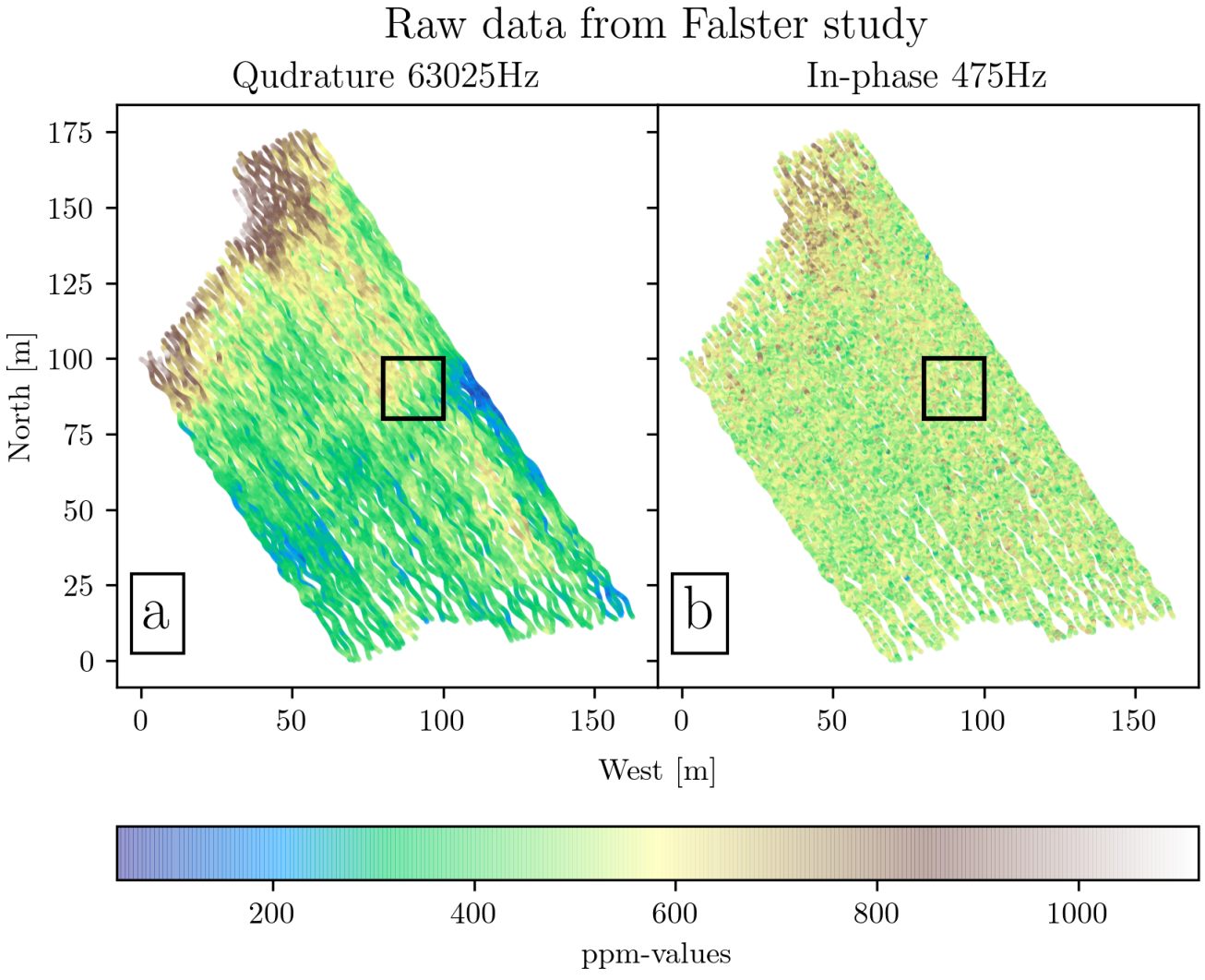

Figure 8. Falster drone-towed CSEM survey. The survey was carried out in T-mode. In (a) quadrature 63025Hz is shown, and in (b) in-phase at 475Hz for quadrature is shown. The black box outlines the sub-area in Figure 9

https://doi.org/10.5194/egusphere-2022-217
Preprint. Discussion started: 12 May 2022

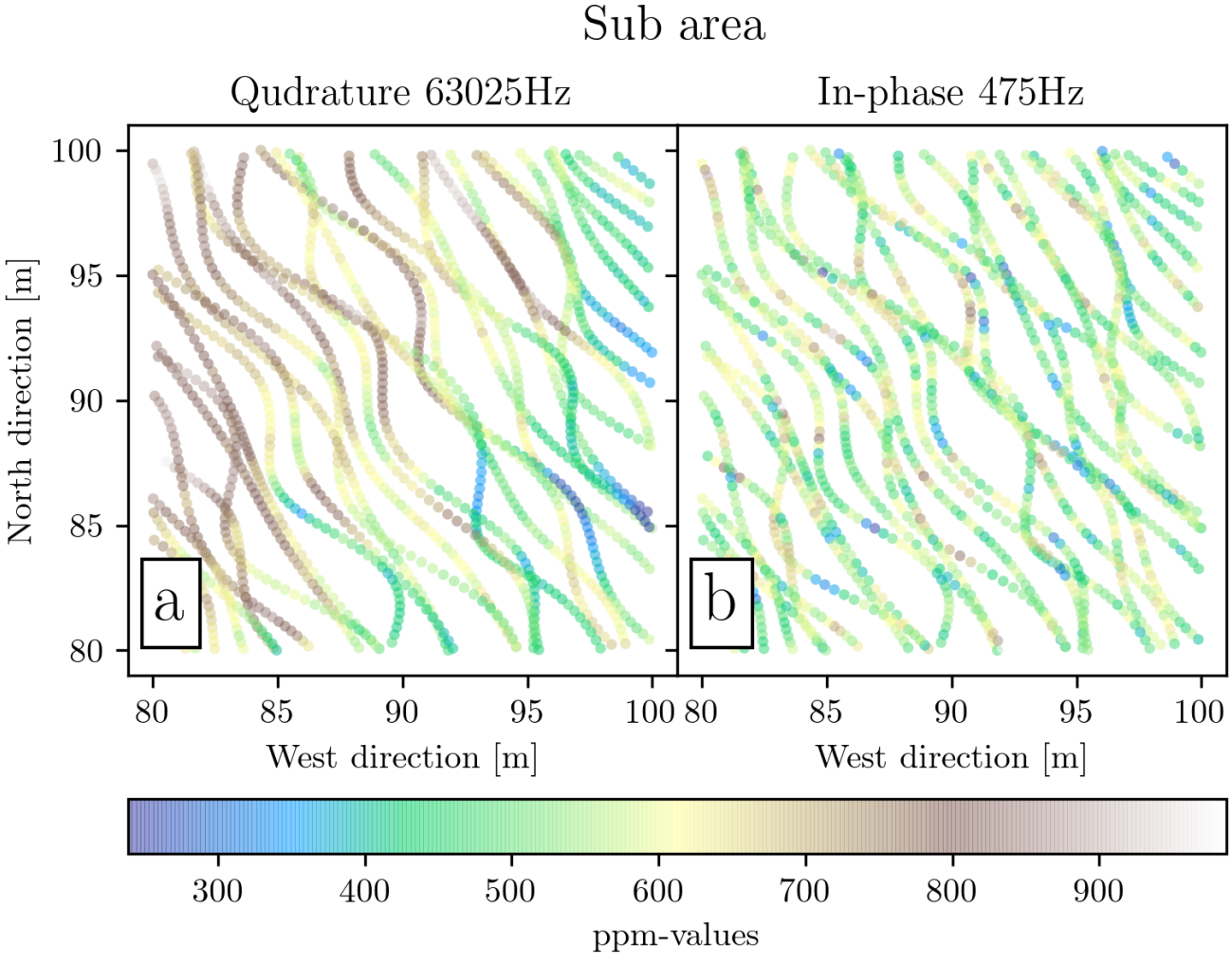

Figure 9. Close up picture of a part of the Falster survey data (see black box in Figure 8). Note the inconsistency in values between adjacent survey lines.

https://doi.org/10.5194/egusphere-2022-217
Preprint. Discussion started: 12 May 2022

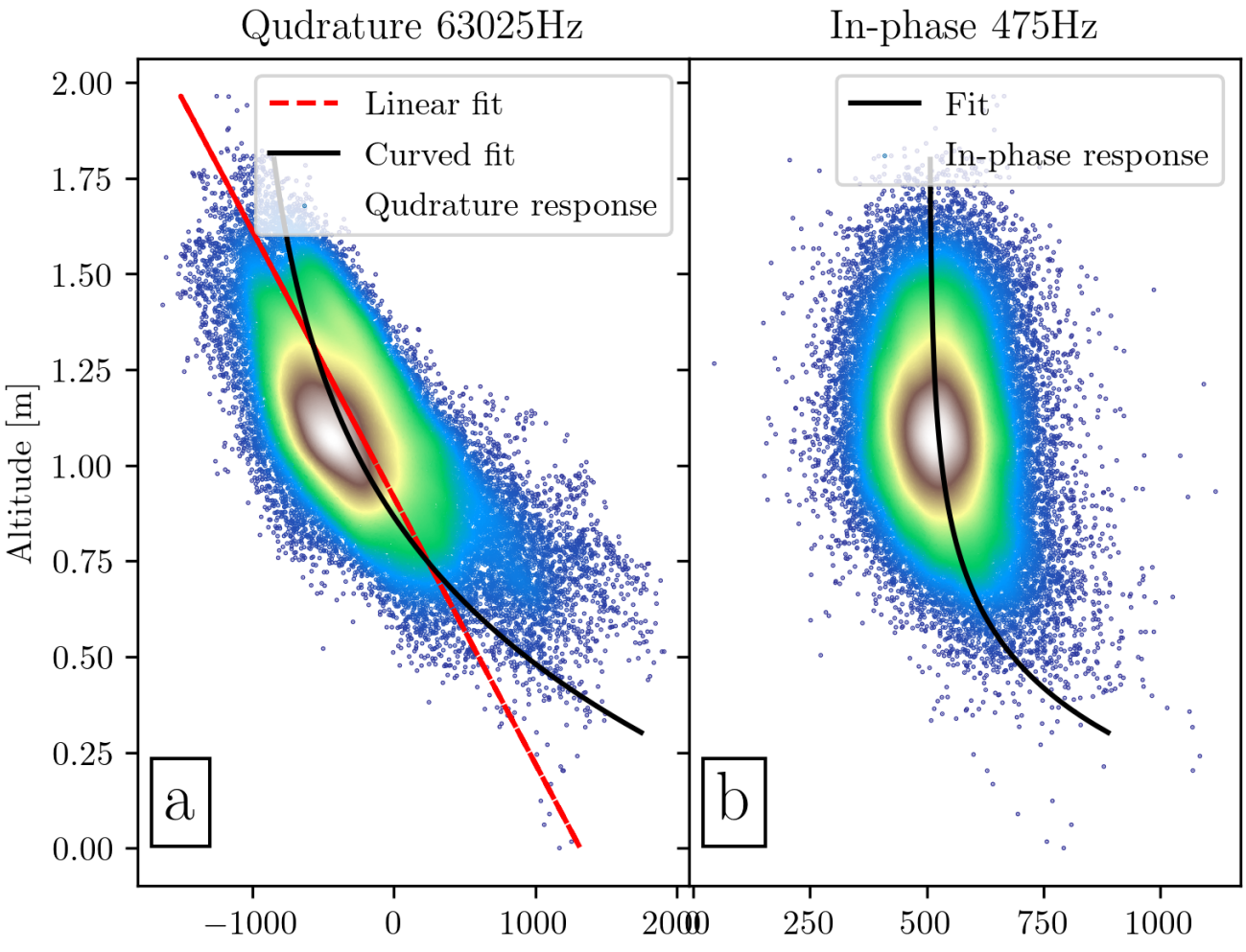

Figure 10. Ppm versus altitude for the Falster survey data shown as scatter-density plot. (a) Quadrature response at 63025Hz; (b) In-phase response at 475Hz. We calculated a fit on the form of $a + b \cdot \exp(h \cdot c)$, represented here as the black line. The parameters a, b, and c in the fit can also be found in Table 3. We further calculated the linear fit for the quadrature response (slope of ∼14ppm/cm; shown with the red line) in order to honor the linear correlation results of the controlled Test 3 in Figure 5.

https://doi.org/10.5194/egusphere-2022-217
Preprint. Discussion started: 12 May 2022

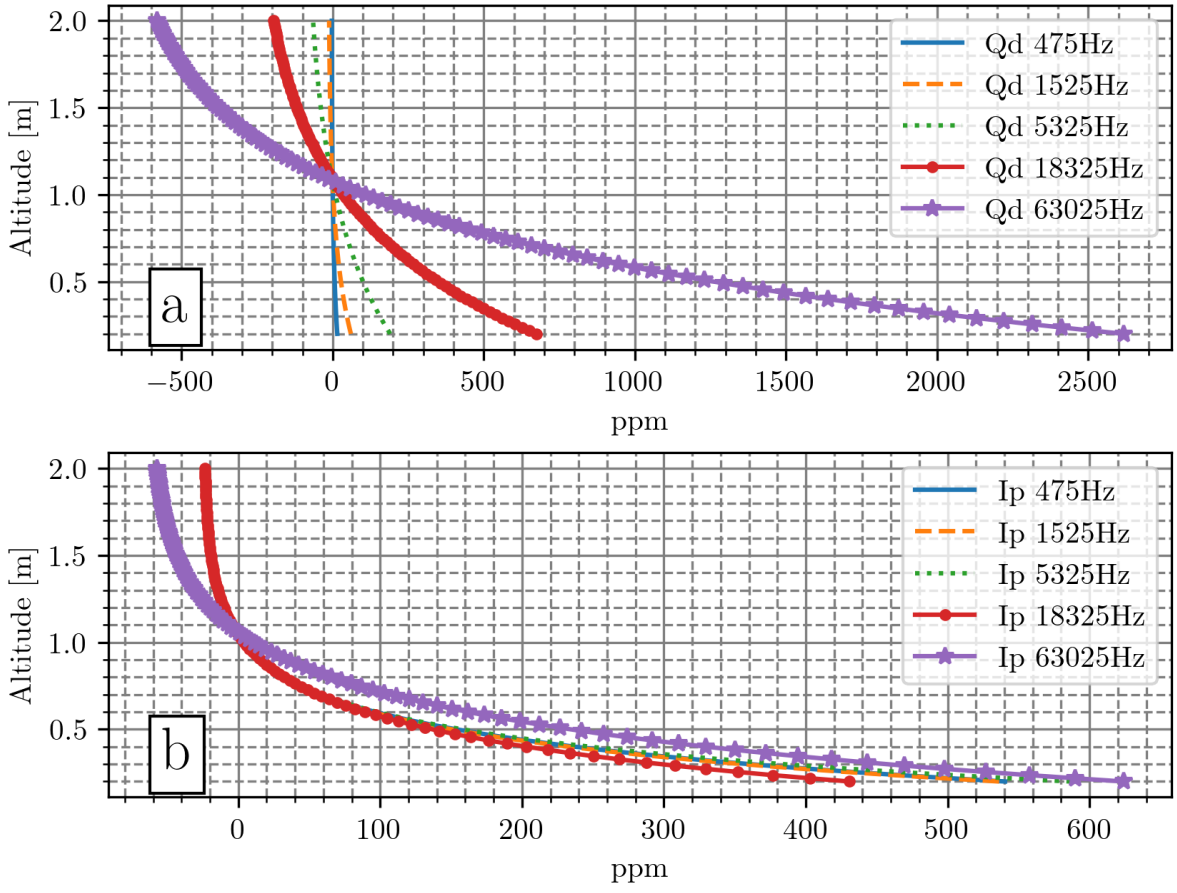

Figure 11. Calculated fits of ppm-values vs altitude for all frequencies of the Falster survey. The parameters a, b, and c are optimised to the smallest least-square misfit for the equations $a + b \cdot \exp(h \cdot c)$ where h is the altitude. All parameters are listed in Table 3.

https://doi.org/10.5194/egusphere-2022-217
Preprint. Discussion started: 12 May 2022

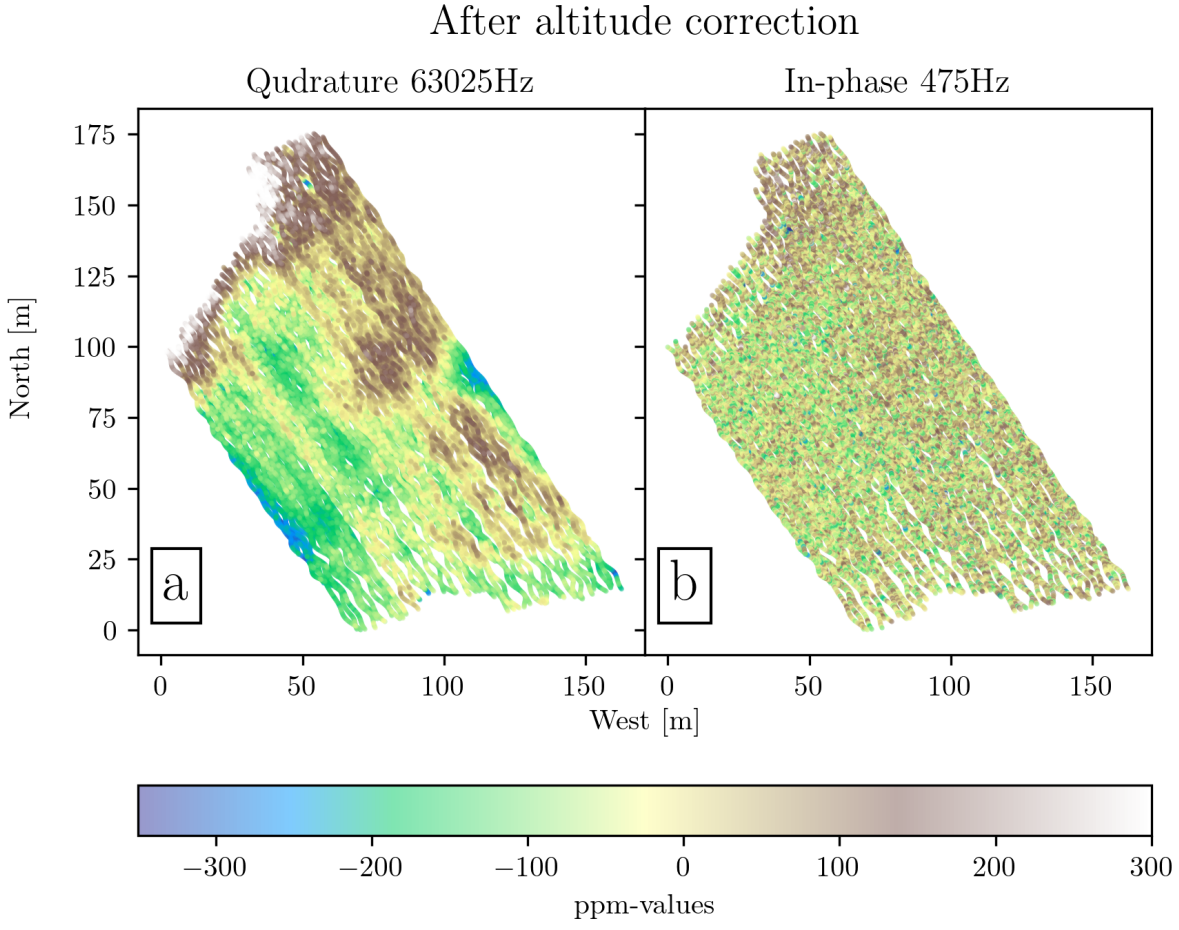

Figure 12. Falster survey data before and after altitude correction. (a) Quadrature response at 63025Hz,(b) Altitude corrected quadrature response at 63025Hz, (c) In-phase response at 475Hz, (d) Altitude corrected in-phase response at 475Hz.

https://doi.org/10.5194/egusphere-2022-217
Preprint. Discussion started: 12 May 2022

	Transmission frequencies:		40.025Hz	65.675Hz	91.275Hz
A	Ppm value per degree [ppm/C^o]	In-phase	9.0	12.0	23.3
		Quadrature	5.6	11.9	32.2
	Transmission frequencies:		40.025Hz	65.675Hz	91.275Hz
B	Ppm value per height [ppm/cm]	In-phase	-16.9	-22.9	-28.6
		Quadrature	-27.6	-37.6	-46.2

Table 1. (A) The estimated temperature effect on ppm-values for 40025Hz, 65675Hz, and 91275Hz. The unit is ppm/C^o, which is calculated from the maximum and minimum values for ppm-values and temperature. (B) The slope of the linear fit from Figure 5.

https://doi.org/10.5194/egusphere-2022-217
Preprint. Discussion started: 12 May 2022

	Drone and CSEM sensor seperation [m]:		0.3	1.0	2.3	3.4	4.2	5.2	6.9	9.2
A	Standard deviation of the 93.075Hz transmission frequency [ppm]	In-phase	559.8	85.7	28.7	21.4	19.8	19.6	20.6	19.7
		Quadrature	173.4	116.9	23.8	22.8	19.4	19.9	20.0	19.9
	Drone and CSEM sensor seperation [m]:		0.3	1.0	2.3	3.4	4.2	5.2	6.9	9.2
B	Standard deviation of the 475Hz transmission frequency [ppm]	In-phase	1234.7	264.8	66.7	58.3	46.8	44.2	45.	44.1
		Quadrature	1288.4	289.5	79.	47.9	48.6	47.8	46.3	43.4
	Drone and CSEM sensor seperation [m]:		0.3	1.0	2.3	3.4	4.2	5.2	6.9	9.2
C	Power line contribution [ppm]	93.075Hz	1.23	0.71	0.44	0.37	0.31	0.24	0.23	0.26
		475Hz	1.19	0.76	0.45	0.39	0.38	0.2	0.25	0.18

Table 2. A collection of values from the Test 6. We can read from the numbers that at around 4.2m to 5.2m, the noise from the drone is no longer visible in the data.

https://doi.org/10.5194/egusphere-2022-217
Preprint. Discussion started: 12 May 2022

	Transmission frequencies:		475Hz	1525Hz	5325Hz	18.325Hz	63.025Hz
A	Standard deviation	In-phase	94.4	73.7	70.7	211.6	93.6
	of Falster study	Quadrature	90.5	61.9	69.7	251.6	478.6
	Transmission frequencies:		475Hz	1525Hz	5325Hz	18.325Hz	63.025Hz
B	Least square fit	a	-3.4	-14.0	-94.1	-270.7	-729.7
	to quadrature response	b	28.0	109.5	366.3	1251.6	4731.1
	$a + b \cdot c^{h \cdot c}$	c	-2.0	-1.2	-1.2	-1.4	-1.7
	Transmission frequencies:		475Hz	1525Hz	5325Hz	18.325Hz	63.025Hz
C	Least square fit	a	-24.9	-21.7	-21.1	-24.3	-61.6
	to in-phase response	b	1219.8	1223.6	1374.3	910.4	1201.2
	$a + b \cdot c^{h \cdot c}$	c	-3.8	-3.9	-4.0	-3.4	-2.8

Table 3. (A) The calculated standard deviation of the Falster survey. The parameters a,b and c shown in Figure 11. Where (B) shows the parameters of the least-square fit for the quadrature response, and (C) shows the parameters of the least-square fit for the in-phase response.